Journal of Molecular Structure 1127 (2017) 377–385

Contents lists available at ScienceDirect

Journal of Molecular Structure

journal homepage: http://www.elsevier.com/locate/molstruc

Experimental and quantum chemical studies on the molecular structure of 3,3,3-trifluoropropane-1-sulfonyl chloride: $CF_3CH_2CH_2SO_2Cl$

J.E. Galván [a, b], M.E. Defonsi Lestard [a, b, 1], M.E. Tuttolomondo [a, b], A. Ben Altabef [a, b, *, 1]

[a] Instituto de Química Física, Facultad de Bioquímica, Química y Farmacia, Universidad Nacional de Tucumán, San Lorenzo 456, T4000CAN Tucumán, R, Argentina
[b] Instituto de Química del Noroeste Argentino, INQUINOA-CONICET-Tucumán, R, Argentina

ARTICLE INFO

Article history:
Received 8 June 2016
Received in revised form
27 July 2016
Accepted 30 July 2016
Available online 2 August 2016

Keywords:
3,3,3-Trifluoropropane-1sulfonyl chloride
Quantum chemical calculations
IR spectroscopy
Raman spectroscopy

ABSTRACT

The experimental and theoretical study on the molecular and vibrational analysis of $CF_3CH_2CH_2SO_2Cl$, 3,3,3-trifluoropropane-1-sulfonyl chloride is presented. The IR and Raman spectra were recorded in liquid state and compared with the spectral data obtained by the DFT/B3LYP method usingthe6-311G(3df) basis set. The influence of hyperconjugation effects of the lone pairs (LP) chlorine atom on the vibrational behavior of the group SO_2 was determined. The TD-DFT approach was applied to assign the electronic transitions observed in the UV–visible spectrum.

1. Introduction

The sulfonyl group has many important applications in organic and medicinal chemistry. As a solid group, it is used for the protection of amines and sulfones [1,2].

Sulfonyl chlorides are often chosen as building blocks in medicinal chemistry for their ability to easily react with heterocyclic amines to create complex sulfonamides [3,4] like 3,3,3-trifluoropropane-1-sulfonyl chloride. Cyclopropanesulfonyl chloride and cyclopentanesulfonyl chloride are reported in detail as building blocks in the synthesis of TNF- converting enzyme (TACE) inhibitors [3].

Structural and conformational properties of several compounds of the YSO_2R type with Y = CF_3,CH_3, $CCl_3$and R = F, OH, NH_2, CH_3, CF_3,Cl, O^-,Na^+ [5–8] were previously studied in this laboratory. The electronic properties and vibrational spectra of 3,3,3-trifluoropropane-1-sulfonyl chloride were not studied previously. Because of the extensive and varied field of application of this compound, we have extended our investigation to the $CF_3CH_2CH_2SO_2Cl$ molecule, to obtain information about the conformational and vibrational properties. The transferability concept is very useful to predict the structure and conformational preference of the compounds of the YSO_2R type by means of quantum mechanical calculations and vibrational analysis. In this paper we present a complete analysis of vibrational spectra (infrared and Raman) obtained from experimental and theoreticalparametersoptimized with different combinations of basis sets.

Besides, the energy of the system in relation to the internal rotation around the CC-SCl dihedral angle was calculated using several computational approaches and fitted to the six-fold Fourier-type expansion. The conformational preference of the molecule can be explained using this methodology.

The UV–visible spectrum of the $CF_3CH_2CH_2SO_2Cl$ in methanol solution was also recorded and electronic property (Frontier orbitals) and band gap energy were calculated by the TD-DFT approach. The influence of hyperconjugation effects of the lone pairs (LP) chlorine atom on the vibrational behavior of the group $SO_2$was studied in the two conformers. The lpCl → σ*S=O interaction incrementis correlated with a decrease of the S=O antisymmetric stretching in all conformers.

* Corresponding author. Instituto de Química Física, Facultad de Bioquímica, Química y Farmacia, Universidad Nacional de Tucumán, San Lorenzo 456, T4000CAN Tucumán, R, Argentina.
E-mail address: altabef@fbqf.unt.edu.ar (A. Ben Altabef).
[1] Member of the Research Career of CONICET.

http://dx.doi.org/10.1016/j.molstruc.2016.07.115
0022-2860/

2. Materials and methods

2.1. Experimental

The $CF_3CH_2CH_2SO_2Cl$ compound was purchased from Sigma-Aldrich Chemical Company with a stated purity greater than 97% and was used without further purification. The FTIR spectrum was recorded in the 4000–400 cm^{-1} region with a spectral resolution of 2 cm^{-1}using a Perkin-Elmer GX1 FTIR spectrometer. The Raman spectrum of the liquid at RT was measured in the4000–100 cm^{-1} interval with a Thermoscientific DXR Raman microscope. The Raman data were collected using a diode-pump, solidstate laser of 532 nm.

The UV–visible absorption spectrum of the $CF_3CH_2CH_2SO_2Cl$ in methanol solution was examined in the 200–400 nm range using a Beckman DU 7500 diode array spectrophotometer.

2.2. Computational details

Quantum-chemical calculations were performed using the Gaussian 03 program package [9]. Geometry optimisations were performed using DFT functionals. Pople's6-31G(d), 6-311G(d,p), 6-311G(3df), 6-311++G(d,p) [10–12] and Dunning correlation consistent cc-pVDZ [13] basis sets were used throughout. DFT calculations were performed using Becke's three-parameter hybrid exchange functional(B3) combined with the Lee-Yang-Parr gradient-corrected correlation functional(LYP) [14–17]. The second DFT method used, mPW1PW91 [18], applies a modified Perdew-Wang exchange functional and Perdew-Wang 91 correlation functional. The gradient-corrected correlation functional of Perdew, Burke and Ernzerhof (PBEPBE) was also used in the geometry optimisations [19,20]. All calculations were performed with standard gradient techniques and default convergence criteria. The nature of stationary points was checked through the vibrational wavenumbers calculated from the analytical second derivatives of the energies, with zero-point energy corrections neglected.

The potential energies associated with dihedral angles were calculated with MP2 [21]. and B3LYP methods using the 6-31G(d), 6-311G(d,p) and 6-311++G(d,p) basis sets where the molecular geometry was optimised for fixed values of the C1-C2-C5-S11 dihedral angle and all other parameters allowed to relax. In a second similar set of calculations, the C2-C5-S11-Cl12 dihedral angle was fixed. The total energy curve was constructed in 10° steps using default convergence criteria as implemented in the Gaussian03 programs.

Vibrational modes were assigned using the GaussView program [22]. The calculated frequencies were scaled using the Yoshida [23] methodology and the potential energy distribution (PED) was calculated using the VEDA program [24].

Electronic transitions within the single-electron approximation and the SCRF, Polarizable Continuum Model (IEF-PCM and C-PCM) approximation in methanol [25–30], were analyzed by the time-dependent DFT (TD-DFT) method. The absorption energies in the UV–visible range with their CI (configuration interaction) description as well as their oscillator strength ($f > 0$) were obtained from vertical electronic excitation energies.

A natural bond orbital (NBO) calculation was performed at the B3LYP/6-311++G(d,p) level using the NBO 3.1 [31–34]program as implemented in the Gaussian 03 package.

The population was calculated according to a Boltzmann distribution:

$$\%pop_i = \frac{e^{-\Delta G_i/RT}}{\sum_{k=1}^{n} e^{-\Delta G_k/RT}} \times 100\% \quad (1)$$

2.3. Prediction of Raman dispersion intensities

The Raman activities (SRa) calculated with Gaussian 03 program were converted to relative Raman intensities (IRa) using the following relationship derived from the theory of Raman scattering intensity [35]:

$$I_i = \frac{f(\upsilon_0 - \upsilon_i)^4 S_i}{\upsilon_i \left[1 - \exp\left(\frac{-hc\,\upsilon_i}{k\,T}\right)\right]} \quad (2)$$

where ν_0 is frequency of the exciting laser light ($\nu_0 = 18797$ cm^{-1} corresponding to the wavelength of 532 nm of a diode-pump, solidstate laser a con-focal aperture of 25 lm pinhole and 10 objective), ν_i is the frequency of the ith normal mode (cm^{-1}) and S_i is the Raman scattering activity of the ith normal mode. f is a suitably chosen common normalization factor for all peak intensities (equal to 10^{-12}).

3. Results and discussion

3.1. Molecular energy and structural properties

The potential energies surface (PES) (Fig. S1) of the $CF_3CH_2CH_2SO_2Cl$ were calculated with PM6 [36] semiempirical methods, with respect to the CCCS and CCSCl dihedral angles. There were eight minima on the potential surface, four of which were the mirror image of the other four (Fig. 1). Since three of them had a free energy difference lower than10 kJ mol^{-1} with respect to the most stable form they were chosen to be studied.

In order to make a comprehensive study of the conformations, other calculations of potential energy variation were made with respect to theCCCS and then with respect tothe CCSC dihedral angles calculated with MP2 and B3LYP methods using different basis sets(Fig. 2(*a*) and (*b*)). There is a good agreement between them in terms of maxima and minima positions, although the B3LYP method gave slightly smaller relative energies. The potential-energy scans of the CCCS dihedral angle showed two minima. One represented the *anti, anti*(*a, a*) (C_s)form (CCCS and CCSCl = 180°) and the other a *gauche, quasi-anti,* (g, q-*a*) (C_1) form (*g, q-a*) (CCCS = 160° and CCSCl = 75.3°). All the groups in both conformers were staggered. The potential-energy scan of the CCSCl dihedral angle identified two minima, the *anti, anti*(*a, a*) (C_s)form (CCCS and CCSCl = 180°) and the *anti, gauche (a, g)*(C_1)form (CCCS = −176.9 and CCSCl = −69.8°). All groups in both conformers were staggered.

In Table 1 the free energy is shown for the above mentioned conformers and the amounts of each conformer that should be observed in the gas phase at room temperature (using the Boltzman distribution equation). The conformer population ratio was predicted to be 1:29:70 (B3LYP/6-311G(3df)) since the free energy differences were $\Delta G_{(a,g\text{-}a,a)}$ = 9.90 kJ mol^{-1} and $\Delta G_{(g,q\text{-}a\text{-}a,a)} = -0.49$ kJ mol^{-1} considering that the *a, g* and *g, q-a* conformers have a double degeneracy relative to the *a, a* conformer. Three conformers are shown in Fig. 1.

3.2. Internal barrier decomposition schemes

The total energy surface for the target torsion angle was

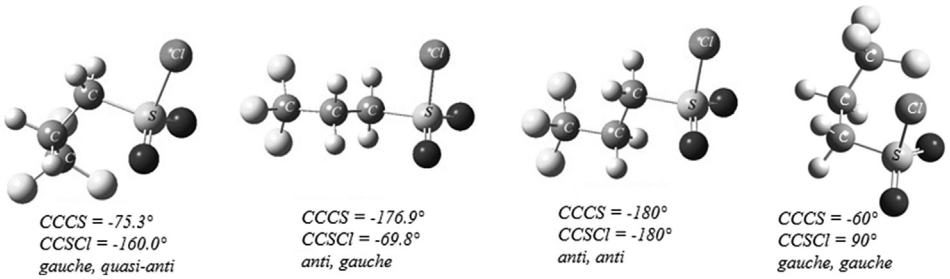

Fig. 1. Calculated molecular structure of the four conformers of $CF_3CH_2CH_2SO_2Cl$.

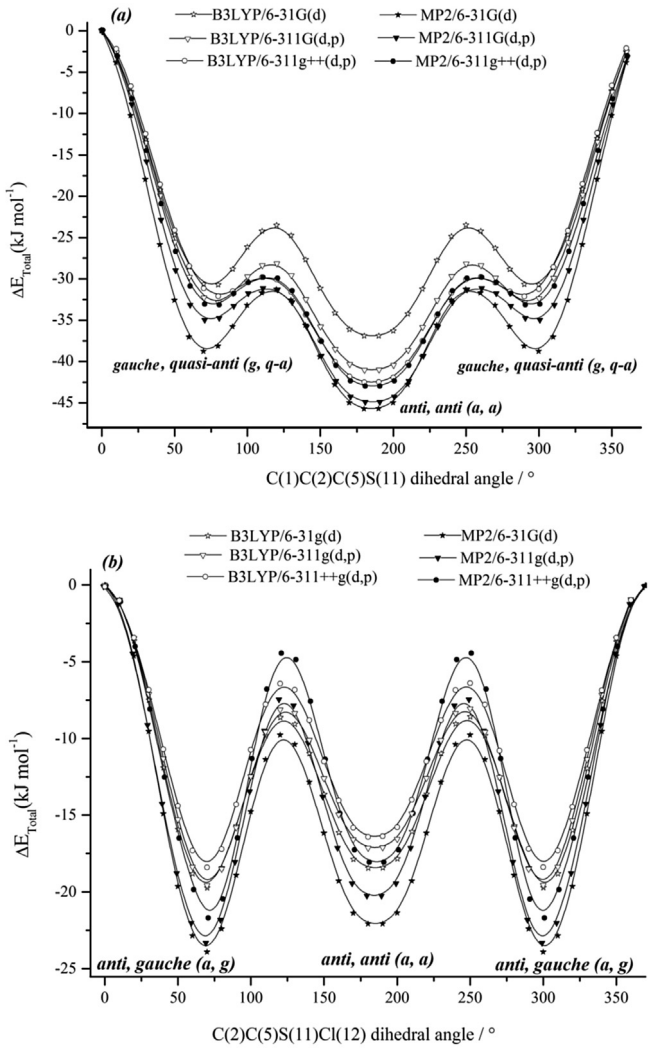

Fig. 2. Torsional potential about *(a)* the C(1)C(2)C(5)S(11) angle and *(b)* the C(2)C(5)S(11)Cl(12) angle of $CF_3CH_2CH_2SO_2Cl$, calculated at different levels of theory.

calculated in steps of 10° in the range 0–180° relaxing all geometrical parameters except for the scanned one. The energy profiles were fitted to a sixth-order Fourier expansion:

$$V(\theta) = \sum_{i=1}^{6} \frac{1}{2} V_{iN}(1 - \cos iN\theta) \quad (3)$$

where *N*, the symmetry number, is equal to 1. No contributions to torsional energies from zero-point energy were taken into account.

Decomposition of the total energy function and analysis of the different terms $V_i$have previously been shown to be a simple way of analyzing the stabilization of different conformations in molecular systems [6,37–42].

Fig. 3 (a) and (b) illustrate the Fourier decomposition of the energy function calculated at the B3LYP/6-311++G(d,p) level for the C(2)C(5)S(11)Cl(12) and C(1)C(2)C(5)S(11) torsions, respectively. Table S1 lists the six V_i terms calculated for $CF_3CH_2CH_2SO_2Cl$ at theB3LYP/6-311++G(d,p) level for both torsions. V_1 and V_3 are the main contribution to the CCCS torsional barrier, while$V_1>V_3>V_2$; V_4-V_6 are less relevant. The large V_1 values show a strong preference of the molecule for the *a, a* conformer over the *g, q-a* one. This means that the conformer would be stabilized by local dipole and steric interactions. The large negative V_3 value indicates that both conformations are stabilized through unfavorable bond-bond eclipsing interactions.

The conjugative and hyperconjugative interactions are represented by theV_2parameter. It is negative, but smaller than V_1, indicating that the contribution of the hyperconjugative effect stabilizes the *g, q-a*conformer, but its value is not high enough to reduce the energy barrier.

The V_3term is import and for the rotation relating to the CCSCl dihedral angle, as shown in Table S1. This term has the same preference for both conformers (*a, a*and *a, g*), whereas the V_1 and V_2 terms prefer the *a, a* and *a,g* respectively.

The balance between V_1 and V_2 (1.35 kJ mol^{-1}) gives us the energy difference between *a,a* and *a,g* forms (1.89 kJ mol^{-1}); while V_3 (12.69 kJ mol^{-1}) gives us the shape of the curve and its value is the energy barrier between conformers (12.11 kJ mol^{-1}) (Fig. 3(b)).

The torsion barrier was characterized using two different schemes to investigate the energetic consequences of the CCSCl and CCCSmoiety rotation. The total energy changes were decomposed as a sum of potential and kinetic contributions in the first one. The natural bond orbital partitioning scheme, NBO, was applied in the second one, to decompose the total energy in the $E_{Lewis}$and E_{deloc} terms. As a first approach, we performed an investigation of the energy barrier based on the partition offered by the scheme:

$$\Delta E = \Delta E_{nn} + \Delta E_{en} + \Delta E_{ee} + \Delta E_k \quad (4)$$

where ΔE stands for the total energy change between structures of different geometries, $\Delta E_{nn}$is the energy change for the nuclear repulsion energy, ΔE_{en} is the energy change for electron-nuclear attraction energy, ΔE_{ee} is the energy change for the electron repulsion energy and ΔE_k is the kinetic energy [43].

Results obtained after applying this partitioning scheme to the energy as a function of the C(2)C(5)S(11)Cl(12) and C(1)C(2)C(5)S(11) torsions at the B3LYP/6-311++G(d,p) level can be visualized in Fig. 4 (a)and(b) respectively.

The *a, a* conformer is favored byE_{ee} and E_{nn} repulsive terms while the E_{en} attractive term favors the other *gauche* forms.

Table 1
Free energies (energies in Hartrees), differences in free energies for three conformers of $CF_3CH_2CH_2SO_2Cl$ at different levels of theory.

Method	Base	G	G	G	$\Delta G_{g\text{-}a}$ [a,b]	$\Delta G_{a.\ g\text{-}a}$ [a]	Relative populations		
		g, q-a	*a, a*	*a, g*			*g, c-a*	*a, a*	*a, g*
B3LYP	6-31G(d)	−1424.98314	−1424.98589	−1424.98611	7.22	−0.57	3	28	69
B3LYP	6-311G(d,p)	−1425.20634	−1425.20972	−1425.21015	8.86	−1.13	1	24	75
B3LYP	6-311++G(d,p)	−1425.22494	−1425.22891	−1425.22932	10.40	−1.07	1	24	75
B3LYP	6-311G(3df)	−1425.29964	−1425.30342	−1425.30361	9.90	−0.49	1	29	70

[a] $\Delta G_{g\text{-}a} = (G_{gauche}\text{-}G_{anti})$, $\Delta G_{a\text{-}g\text{-}a} = (G_{anti,\ gauche}\text{-}G_{anti})$.
[b] ΔG in kJ mol^{-1}.

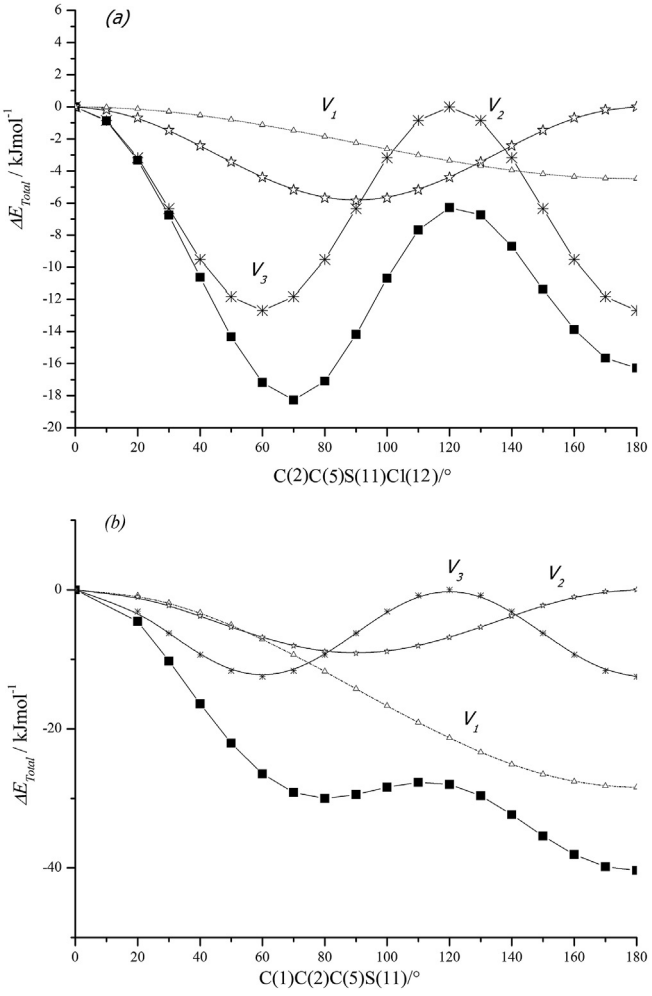

Fig. 3. Fourier decomposition of the potential function for V(θ) $CF_3CH_2CH_2SO_2Cl$ for (a) the C(2)C(5)S(11)Cl(12) and (b) C(1)C(2)C(5)S(11) dihedral angles calculated using the B3LYP method with 6−311++G(d,p) basis set by the decomposition of the total energy function and the different V_i terms.

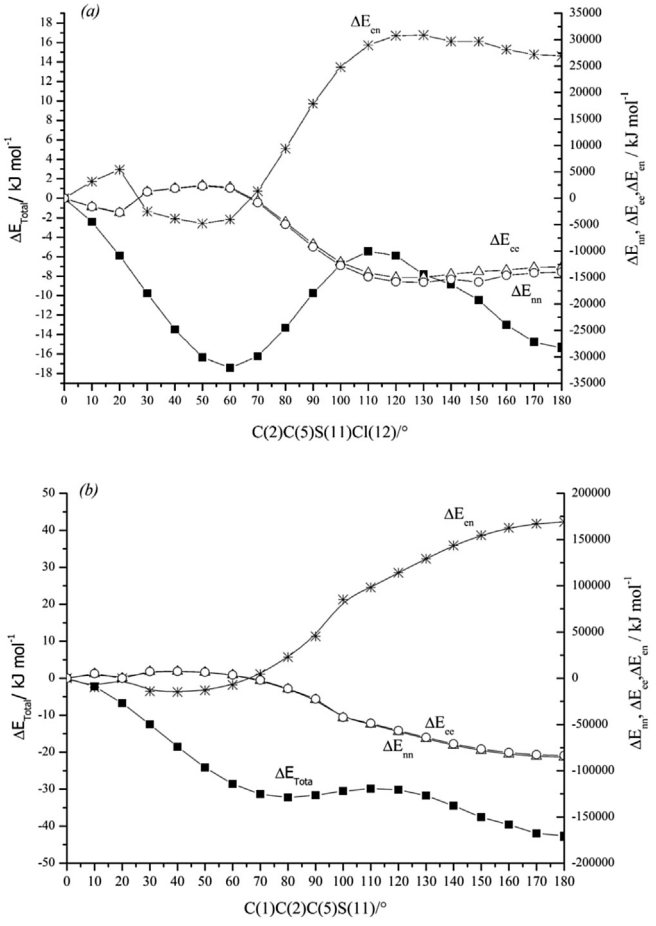

Fig. 4. Dependence of attractive (ΔE_{ne}) and repulsive (ΔE_{nn} and ΔE_{ee}) energy increments on the (a) C(2)C(5)S(11)Cl(12) and (b) C(1)C(2)C(5)S(11) dihedral angles of $CF_3CH_2CH_2SO_2Cl$ calculated at the B3LYP/6-311++G(d,p) level.

On the basis of the natural bond orbital method, NBO,a complementary analysis of the barrier [38,41] can be performed according to Equation (5) by analyzing the Lewis and hyperconjugative (non-Lewis) terms:

$$\Delta E_{barrier} = \Delta E_{Lewis} + \Delta E_{deloc} \quad (5)$$

where δe_{lewis} represents the energy of the hypothetical localized species described by a determinant of nearly doubly occupied NBOs comprising the core, lone-pairs and localized bonds of the Lewis structure. The delocalization energy change, ΔE_{deloc}, represents the hyperconjugative stabilization contribution to the rotational barrier that arises from bond→antibonding charge transfer [38–43].

Fig. 5(a) presents the contributions of the localized electron density (E_{Lewis}) and the delocalized electron density (E_{deloc}) to the CCCStorsion barriers at the B3LYP/6-311++G(d,p) level. The Lewis energy is decisive for the energetic preference; its minima correspond to the *a*, *a* and *g, q-a*conformers. This result agrees with the value of V_1 in the decomposition potential energy. When electron delocalization is not taken into account, the steric effect in both conformers is dominant, but greater in the *a, a* conformer(see Table S2 and S3).

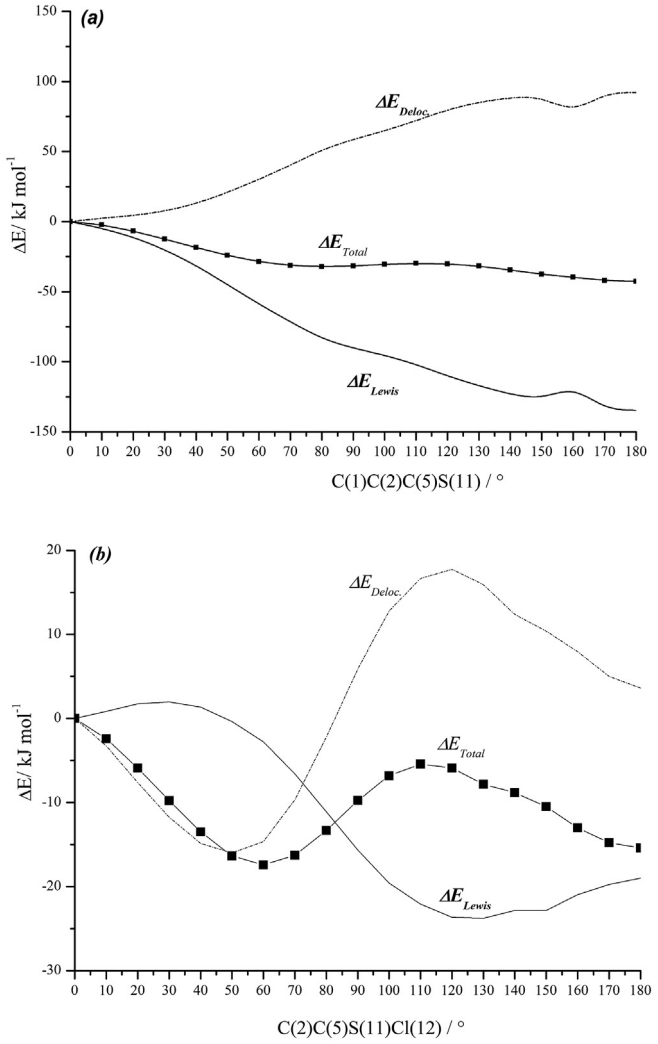

Fig. 5. Dependence of the relative total energy of the $CF_3CH_2CH_2SO_2Cl$ molecule and its $\Delta E_{Lewis}$and ΔE_{deloc} parts on the (a) C(1)C(2)C(5)S(11) and (b) C(2)C(5)S(11)Cl(12) rotation angles at B3LYP/6-311++G(d,p) level.

Fig. 5(b) shows that the delocalization energy difference, ΔE_{deloc}, is greater for the *a,g* conformer than for the *a*, *a* conformer. This effect of the *a,g* structure in $CF_3CH_2CH_2SO_2Cl$ can be explained by orbital interactions between the Cl lone pairs (lp Cl) and the vicinal antibonding orbitals (Table 2).

3.3. Electronic excitations and UV–visible analysis

The UV–visible spectra measured in methanol solution were compared with quantum calculations carried out with TD-DFT method usingTD-B3LYP, TD-PBEPBE and TD-mPW1PW91 functionals and 6-311++G(d,p) and cc-pVDZ basis sets in implicit solvent using IEF-PCM and C-PCM models [25–29]. The results are presented in Table S6 and can be seen in Fig. S2. Both methodologies give the same results, as expected for that solvent polarity [29]. What is observed is a major deviation from the change of functional, but not for the basis set change (Fig. S3).

The λ_{max} values obtained from the UV–visible spectra were analyzed with the rmPW1PW91/cc-pVDZ level of theory, because with this functional the least deviation is obtained with respect to the experimental spectrum [30]. In Table 3 the calculated UV absorption maxima, theoretical electronic excitation energies and

Table 2
Relevant hiperconjugative interactions calculated at B3LYP/6-311++G(d,p) level using NBO analysis.

Donor (*i*) → Acceptor (*j*) interaction[a]	E(2)[b]		
	a, g	*a, a*	*g, q- a*
LP(2)Cl(12) → σ*S(11)–O(13)	14.50	11.87	5.02
LP(2)Cl(12) → σ*S(11)–O(14)	6.23	12.12	14.34
LP(3)Cl(12) → σ*C(5)–S(11)	5.85	6.10	4.68
LP(3)Cl(12) → σ* S(11)–O(13)	–	3.64	9.61
LP(3)Cl(12) → σ* S(11)–O(14)	8.32	3.34	–
LP(3)Cl(12) → σ*C(2)–C(5)	–	3.97	3.09
LP(1)O13 → σ*C(5)–S(11)	3.55	3.80	3.55
LP(1)O13 → σ*S(11)–Cl(12)	2.26	2.51	2.34
LP(1)O13 → σ* S(11)–O(14)	7.90	7.36	7.61
LP(2)O13 → σ*C(5)–S(11)	61.57	58.73	61.74
LP(2)O13 → σ* S(11)–O(14)	70.51	72.48	70.10
LP(3)O13 → σ*S(11)–Cl(12)	174.26	172.59	174.89
LP(3)O13 → σ* S(11)–O(14)	14.46	14.04	15.34
LP(3)O13 → σ* C(5)–S(11)	11.08	12.41	11.16
LP(1)O14 → σ*C(5)–S(11)	3.64	3.80	4.31
LP(1)O14 → σ*S(11)–O(13)	7.86	7.36	8.03
LP(1)O14 → σ*S(11)–Cl(12)	2.34	2.51	2.13
LP(2)O14 → σ*C(5)–S(11)	57.85	58.65	62.03
LP(2)O14 → σ*C(2)–C(5)	2.76	–	2.76
LP(2)O14 →σ*S(11)–O(13)	72.28	72.56	74.86
LP(3)O14 → σ*S(11)–Cl(12)	176.40	172.59	179.57
LP(3)O14 → σ*S(11)–O(13)	14.42	13.92	12.99
LP(3)O14 → σ*C(5)–S(11)	11.45	12.46	12.96
Total	729.49	728.81	743.11

[a] See Fig. S1 for atoms numbering. LP denotes lone pair on the specified atom.
[b] E(2) means energy of hyper-conjugative interactions in kcal mol^{-1}.

oscillator strengths are detailed for both conformers that present the same energies. Fig. 6 shows the predicted experimental and theoretical UV–visible spectra; Table S4 reports the line width parameter used for simulation. As seen in Table 3, the calculated absorption maxima values for the most stable (*a, a)* conformer of the $CF_3CH_2CH_2SO_2Cl$; were 232, 211 and 209 nm. The *f* oscillator strengths are in the 0.002–0.009 range. Transitions with extremely low or zero *f* values are forbidden.

The oscillator strengths for the transition at 209 and 211 nm were higher in magnitude than the other transitions and their corresponding experimental value was observed at 207 and 211 nm. The absorption band at 209 nm was assigned to the transition from the HOMO-3 to LUMO molecular orbital. The maximum absorption located at 211 nm in the calculated spectrum ($f = 0.0042$) was assigned to the HOMO-1/2 → LUMO transitions. The wavelength calculated at 232 nm ($f = 0.0026$) was mainly generated by excitations from the HOMO to LUMO molecular orbital. This transition appeared experimentally as a shoulder at 219 nm(Fig. 6).

3.4. Vibrational analysis

The assignment of the experimental bands to the normal modes of vibration of $CF_3CH_2CH_2SO_2Cl$ was based on comparison with data for related molecules [5–8,44–49] and with the results of the calculations. Fig. 7 (a) and 7(b) show the experimental and calculated IR and Raman spectra, respectively. The observed band positions in the IR and Raman spectra together with calculated wavenumbers and mode assignments PED are collected in Table 4.

The conformationally averaged IR spectrum was simulated by summing the population-weighted spectra for the *a, g, g, q-a*and*a, a*conformers calculated using B3LYP/6-311G(3df) [50,51] wavenumbers and intensities with Lorentzian band shapes ($\gamma = 2\ cm^{-1}$). The populations were calculated with the B3LYP/6-311G(3df) total energy difference using Boltzmann statistics for 1%, 29% and 70%

Table 3
Theoretical electronic absorption spectra of $CF_3CH_2CH_2SO_2Cl$ calculated at mPW1PW91/cc-pVDZ level of theory in methanol solution.

Excited state	Wavelength (nm)			Oscillator strengths (*f*)		Assignment[a]
	Experimental	Calculated				
		a, a[b]	*a,g*[b]	*a, a*[b]	*a,g*[b]	
S1	219	232	230	0.0026	0.0031	HOMO → LUMO
S2	211	211	210	0.0042	0.0056	HOMO-1 → LUMO HOMO-2 → LUMO
S3	207	209	207	0.0050	0.0093	HOMO-3 → LUMO

[a] Experimental UV–visible spectrum measured in methanol solution.
[b] *anti, anti* (*a, a*) (C_s); *anti, gauche* (*a, g*) (C_1).

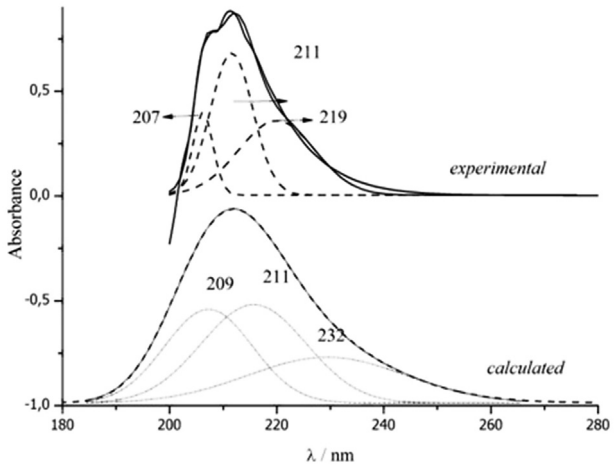

Fig. 6. Calculated and experimental UV–visible spectra for the *a, a* conformer of $CF_3CH_2CH_2SO_2Cl$.

abundance of the three conformers, respectively.

At room temperature, most bands are attributable to the same fundamental for both conformations. The IR and Raman spectra demonstrate the presence of *a, g*and *a, a* conformers by the resolution of several fundamental modes of vibration(Fig. 8(a,b)). Vibrational analyses were performed for the three conformers, but as population of *g, q-a*conformer is much lower than that of the other two, it is not observable in the IR and Raman spectra.

The DFT (B3LYP functional) calculations reproduced the normal frequencies of vibration with the following RMSD (root mean square deviation) values for each basis set for *a, a* and *a, g* forms respectively: 60.4–50.1 cm^{-1} for 6-31G*, 50.8–50.0 cm^{-1} for 6-311G**, 50.5–48.5 for 6-311G(3df) and 50.7–50.0 cm^{-1} for 6-311++G**.Table S5 shows the RMSD for the different regions of the spectrum.

The minor RMSDwere obtained with the combination B3LYP/6-311G(3df). Hence, they were used for the vibrational analysis. We scaled the frequencies calculated with B3LYP/6-311G(3df) with the Yoshida et al. [19] equation (6), giving a *RMSD* value of20.6 and 20.5 cm^{-1} for the *a,a* and *a, g* forms, respectively (Table S5).

$$\upsilon_{obs}/\upsilon_{calc} = 1.0087(9) - 0.0000163(6)\upsilon_{calc} \quad (6)$$

where υ_{obs} and υ_{calc} are given in cm^{-1}, and the errors, given in parentheses, apply to the last significant figure. The ratio $\upsilon_{obs}/\upsilon_{calc}$ in eq. (6) is denoted as the wavenumber scale factor to be applied to the B3LYP/6-311G(3df) calculation.

The wavenumbers calculated with this method for the 36 modes

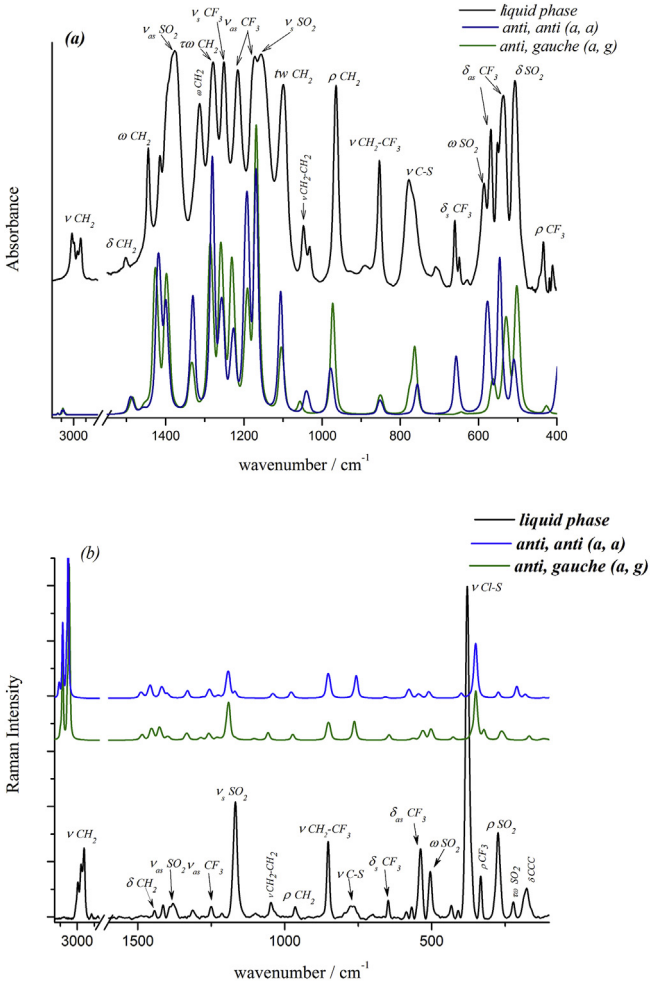

Fig. 7. Experimental and theoretical (a) infrared and (b) Raman spectra of the liquid phase of $CF_3CH_2CH_2SO_2Cl$.

of vibration of $CF_3CH_2CH_2SO_2Cl$ for the bothconformers appear in Table 4, where they are compared with the measured values.

The bands at 1414 and at 1391 cm^{-1} in the Raman spectrum are assigned to the wagging modes of the methylene group showing the presence of *a, g* and *a, a*conformers, respectively.

The symmetric bending of CF_3 group is observed at 647 cm^{-1}in the Raman spectrum. This band also appears to be split into two components in the infrared spectrum showing the presence of *a, a*and*a,g* conformers. This observation is in agreement with the calculations (Fig. 8(b)). The bands at 571 and 552 cm^{-1}(IR spectrum) are assigned tothe antisymmetric bending of theCF_3 group for the *a,g* and *a, a*conformers respectively (difference between

Table 4
Comparison of experimental infrared and Raman wavenumbers (cm^{-1}) with theoretical (harmonic and scaled) wavenumbers (cm^{-1}) and mode assignments PED (%) for the $C_{a,a}$ and $C_{a,g}$ conformers.

Mode	Experimental		Calculated[a] unscaled		Calculated scaled[b]		PED (%)[c]
	IR[d]	Raman[e]	$C_{a,a}$	$C_{a,g}$	$C_{a,a}$	$C_{a,g}$	
1	3013 w	–	3161	3148	3025	3014	90 υ_{as} C(5)H_2 + 10 υ_{as}C(2)H_2
2	2996 w	2995 (13)	3129	3130	2997	2998	90 υ_{as}C(2)H_2
3	2968 w	2967 (28)	3095	3086	2966	2958	89 υ_sC(5)H_2 + 11 υ_sC(5)H_2
4	2942 w	2940 (23)	3080	3070	2952	2943	89 υ_sC(2)H_2 + 11 υ_sC(5)H_2
5	1460sh	1457 sh	1488	1486	1465	1463	84 δ C(2)H_2 + 12 ωC(2)H_2
6	1445 m	1443 (3)	1458	1453	1437	1431	89 δ C(5)H_2
7	1415 m (*a,g*)	1414 (6)		1425		1404	55 ωC(2)H_2
	1393 sh(*a,a*)	1391 (6)	1418		1397		51 ωC(2)H_2
8	1377 s	1381 (6)	1398	1397	1378	1377	94 $\upsilon_{as}SO_2$
9	1314 m	1314 (2)	1332	1333	1214	1316	62 tw C(2)H_2
10	1281 m	–	1281	1285	1265	1270	55 ωC(5)H_2
11	1250 m	1250 (1)	1256	1257	1250	1243	37 υ_s CF_3 + 18 ω C(2)H_2 + 15 ω C(5)H_2 + 10 δ_{as} CF_3
12	1215 m	1215(2)	1228	1229	1213	1216	47 tw C(5)H_2
13	1172 s	1169 (33)	1193	1192	1180	1179	91υ_s SO_2
14	1156 s	–	1169	1167	1157	1155	59 $\upsilon_{as}CF_3$
15	1099 s	1099 (1)	1106	1103	1096	1093	30 $\upsilon_{as}CF_3$ + 29 ρC(2)H_2
16	1049 w (*a,g*)	1042 (4)		1057		1048	79 υC(2)C(5)
	1032 w (*a,a*)	1032 sh	1040		1031		80 υC(2)C(5)
17	966 vs	966 (4)	977	972	970	965	36 ρC(2)H_2+33 $\upsilon_{as}CF_3$
18	854 s	854 (23)	851	850	850	846	79 υC(1)C(2)
19	796 sh	–	786	774	783	771	60 ρCH_2 + 18τ CF_3
20	778 m(*a,g*)	774 (5)		762		760	53 υ S-C+12 δ CCC
	764 sh(*a,a*)	763 (5)	757		755		56 υ S-C + 12 δ CCC
21	661 m (*a,a*)		656		657		30 $\delta_s CF_3$ + 10 υ CS
	649 w (*a,g*)	647 (8)		645		645	46 $\delta_s CF_3$ + 10 υ CS
22	586 m (*a,a*)	585 (7)	577		577		28 ωSO_2 + 23 δ_{as} CF_3
23	571 s (*a,g*)	568 (9)		563		563	26 δ_{as} CF_3 + 18ρ CF_3
	552 m(*a,a*)	552 sh	545		545		33 δ_{as} CF_3 + 14 υ CF_3+ ω11 SO_2
24	537 s	538 (25)	538	537	538	537	62 δ_{as} CF_3 + 19 ρ CF_3
25	510 sh(*a,g*)			529		528	56 δSO_2 + 12 ωSO_2 + 10 υ SCl
	507 m(*a,a*)	505 (18)	509		509		73 δSO_2
22′	490 sh(*a,g*)	495 sh		501		501	33 ωSO_2 + 12 δSO_2
26	434 w (*a,g*)	433 (8)		426		427	29δ_{as} CF_3 + 28 ρ CF_3
	411w (*a,a*)	409 (8)	400		401		58 ρCF_3
27	404 vw	403 sh	372	362	372	363	52 ρCF_3 + 18 $\delta_s CF_3$
28	–	379 (100)	351	349	352	350	68 υ SCl
29	–	333 (18)	342	321	343	322	59 ρSO_2
30	–	276 (27)(*a,a*)	273		274		79 twSO_2
		266 sh(*a,g*)		263		264	
31	–	222 (5)	211	255	212	256	61 δ ClSC
32	–	184 sh	180	169	181	168	47 δ CCC + 17 υ S-C + 16ω SO_2
33	–	177 (9)	120	122	121	123	79 δ CCS
34	–	–	88	109	88	110	83 τ CS
35	–	–	54	53	54	53	80 τ CF_3
36	–	–	36	33	36	33	89 τ C(2)C(5)

ν, stretching; δ bending; ρ rocking; ω wagging; τω twisting.
[a] Calculated at B3LYP/6-311G++(d,p).
[b] Scaled with Yoshida equation [23].
[c] See Table S6 for definition of natural internal coordinates.
[d] s, strong; m, medium; w, weak; sh, shoulder; v, very.
[e] Relative intensity in parentheses.

wavenumbers: experimental, 19 cm^{-1}; theoretical, 18 cm^{-1}). The pair of bands at 433 and 409 cm^{-1} in the Raman spectrum are assigned to the CF_3 rocking modes for the *a,g* and *a, a*conformers (difference between wavenumbers: experimental, 27 cm^{-1}; theoretical, 26 cm^{-1}).

The CH_2-CF_3 stretching mode appears as a medium band in the IR and Raman spectra located at 854 cm^{-1}. The weak bands at 1049 and 1032 cm^{-1} CH_2-CH_2 correspond to the stretching mode for the *a, g* and *a, a* conformers, respectively. This observation is in agreement with the calculation (Fig. 8(a)). The strong band located at 379 cm^{-1} in the Raman spectrum is assigned to the S-Cl stretching mode for bothconformers.

Two strong infrared bands, at 1377 and 1172 cm^{-1}, are assigned to the SO_2antisymmetric and symmetric stretching modes, respectively. The SO_2 bending mode is located at 510 and 507 cm^{-1}(IR spectrum) for the *a, g* and *a, a* conformers, respectively. In the first case they appear mixed with the ω SO_2 and υ SCl. The ωSO_2 mode corresponding to the *a, a* and *a, g* conformers are located at 586 and 490 cm^{-1}(IR spectrum) respectively.

The behavior of hyperconjugative interactions of the different conformers and their relationship to vibrational properties is studied with the NBO program.

Table 2 shows the most important hyperconjugative interactions at the B3LYP/6-311++G(d,p) level. The electronic charge transferred to the chlorine lone pair (lp Cl) is greater for the *a, a* and *g, q-a* form than for the other one. Thus, the lpCl(12) → σ* S(11)-O(13) interaction takes a value of 9.61 and 3.47 kJ mol^{-1} for the *g, q-a* and *a, a* form respectively. Besides, the hyperconjugation of the

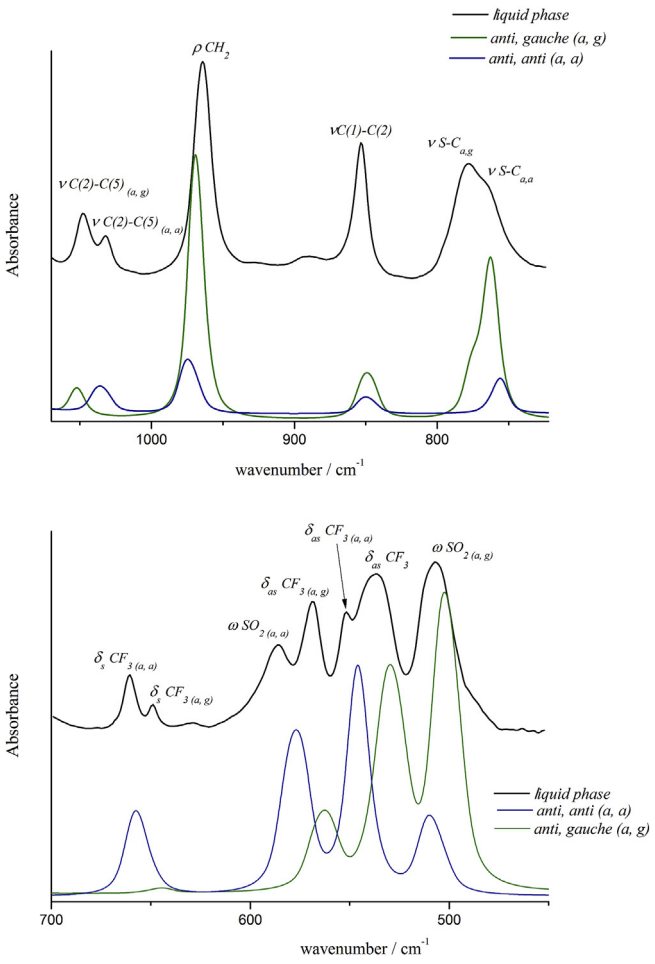

Fig. 8. Experimental and calculated infrared spectra from B3LYP/6-311G(3df) wavenumbers using Lorentzian band shapes: (a) region between 1100 and 720 cm^{-1} and (b) region between 750 and 400 cm^{-1}.

oxygen lone pair (lp O) to the σ*S(11)-Cl(12) and σ*C(5)-S(11) has a higher value for the *g, q-a* than for the other forms. (See Fig. S4 for atom numbers). The lpCl → σ*S═O interaction increment is correlated with a decrease of the *S═O* antisymmetric stretching for the conformer. According to this ratio, it would be υ_{as} *SO2(a, a)* < υ_{as} *SO2 (g, q-a* < υ_{as} *SO2 (a, g)*. The lp(2)Cl(12) → σ*S(11)-O(14) and lp(3) Cl(12) → σ*C(5)-S(11) interactions strengthen the S-Cl bond. This is reflected in a *S-Cl (a, a)* < S-Cl *(g, q-a))* vibration frequency increase and a C-S *(a, a)* > C-S *(g, q-a)* vibration frequency decrease.

4. Conclusions

The optimized molecular geometry and conformations for $CF_3CH_2CH_2SO_2Cl$ were calculated using MP2 and DFT techniques and different basis sets. The structural results showed that the preferred forms were the *a,g,* and *a, a* conformers. As the difference in free energy was calculated at 10.4 kJ mol^{-1} and -1.07 kJ $mol^{-1}$for *a, g* and g, *q-a* conformers relative to *a, a* conformer, respectively, and as the *a, g* and *g, q-a*conformers have a double multiplicity relative to the *a, a* conformer, the ratio population between the three conformers was predicted to be 1:29:70. In order to investigate the energetic consequences of the CCCS and CCSCl moiety rotation, the torsion barrier was characterized. The repulsive terms E_{ee} and E_{nn}, favor the *a, a* conformer while the attractive term E_{en} favors the other forms, being this latter contribution much greater for the *g, q-a* conformer than for the *g, a* one.

The delocalization energy difference, ΔE_{deloc}, is greater for the *a,g* conformer than for the *a, a* conformer in the NBO analysis of the CCSCl torsion barriers. This effect of the *a, g* structure in $CF_3CH_2CH_2SO_2Cl$ can be rationalized by orbital interactions between the sulfur lone pairs (lp Cl) and the vicinal antibonding orbitals. The relatively high $\Delta E_{HOMO-LUMO}$ value indicates that the molecule presents high chemical stability and low reactivity. The IR and Raman spectra demonstrate the presence of *a, g* and *a, a* conformers by the resolution of several fundamental modes of vibration. Vibrational analyses were performed for the three conformers, but as the population of the *g, q-a* conformer is much lower than those of the other two conformers, it was not observable in the IR and Raman spectra.

The differences in the S═O, S-Cl and S-C stretching bands of the two majority conformers clearly justify hyperconjugative interactions where the stereochemistry of the Cl atom in the molecule is fundamental for interaction preferences.

Acknowledgments

This work was supported by SCAIT (D542/2), CONICET (PIP 0205) and ANPCyT (PICT0697).

Appendix A. Supplementary data

Supplementary data related to this article can be found at http://dx.doi.org/10.1016/j.molstruc.2016.07.115.

References

[1] N.S. Simpkins, Sulphones in Organic Synthesis, Pergamon Press, Oxford, England, 1993.
[2] P.D. Magnus, Tetrahedron 33 (1977) 2019.
[3] J.S. Condon, D.J. Mc Carthy, J.I. Levin, H.G. Lombart, F.E. Lovering, L. Sun, W. Wang, W. Xua, Y. Zhang, Bioorg. Med. Chem. Lett. 17 (2007) 34.
[4] D.R. Marshall, G. Rodríguez, D.S. Thomson, R. Nelson, A. Capolina, Bioorg. Med. Chem. Lett. 17 (2007) 315.
[5] L.E. Fernández, A. Ben Altabef, E.L. Varetti, J. Mol. Struct. 612 (2002) 1.
[6] M.E. DefonsiLestard, L.A. Ramos, M.E. Tuttolomondo, S.E. Ulic, A. Ben Altabef, Spectrochim. Acta Part A Mol. Biomol. Spectrosc. 96 (2012) 332.
[7] L.C. Ducati, M.P. Freitas, C.F. Tormena, R. Rittner, J. Mol. Struct. 800 (2006) 45.
[8] M.E. Tuttolomondo, O.E. Piro, E.L. Varetti, A. Ben Altabef, Z. Anorg. Allg. Chem. 632 (2006) 1501.
[9] M.J. Frisch, G.W. Trucks, H.B. Schlegel, G.E. Scuseria, M.A. Robb, J.R. Cheeseman, J.A. Montgomery Jr., T. Vreven, K.N. Kudin, J.C. Burant, J.M. Millam, S.S. Iyengar, J. Tomasi, V. Barone, B. Mennucci, M. Cossi, G. Scalmani, N. Rega, G.A. Petersson, H. Nakatsuji, M. Hada, M. Ehara, K. Toyota, R. Fukuda, J. Hasegawa, M. Ishida, T. Nakajima, Y. Honda, O. Kitao, H. Nakai, M. Klene, X. Li, J.E. Knox, H.P. Hratchian, J.B. Cross, C. Adamo, J. Jaramillo, R. Gomperts, R.E. Stratmann, O. Yazyev, A.J. Austin, R. Cammi, C. Pomelli, J.W. Ochterski, P.Y. Ayala, K. Morokuma, G.A. Voth, P. Salvador, J.J. Dannenberg, V.G. Zakrzewski, S. Dapprich, A.D. Daniels, M.C. Strain, O. Farkas, D.K. Malick, A.D. Rabuck, K. Raghavachari, J.B. Foresman, J.V. Ortiz, Q. Cui, A.G. Baboul, S. Clifford, J. Cioslowski, B.B. Stefanov, G. Liu, A. Liashenko, P. Piskorz, I. Komaromi, R.L. Martin, D.J. Fox, T. Keith, M.A. Al-Laham, C.Y. Peng, A. Nanayakkara, M. Challacombe, P.M.W. Gill, B. Johnson, W. Chen, M.W. Wong, C. González, J.A. Pople, Gaussian 03, Revision C.02, Gaussian, Inc., Wallingford, CT, 2004.
[10] R. Krishnan, J.S. Binkley, R. Seeger, J.A. Pople, J. Chem. Phys. 72 (1980) 650.
[11] A.D. McLean, G.S. Chandler, J. Chem. Phys. 72 (1980) 15639.
[12] M.J. Frisch, J.A. Pople, J.S. Binkley, J. Chem. Phys. 80 (1984) 3265.
[13] D.E. Woon, T.H. Dunning Jr., J. Chem. Phys. 98 (1993) 1358.
[14] A.D. Becke, J. Chem. Phys. 98 (1993) 5648.
[15] (a) C. Lee, W. Yang, R.G. Parr, Phys. Rev. B 37 (1988) 785;
(b) W.J. Hehre, PvR. Scheyer, J.A. Pople, Ab initio Molecular Orbital Theory, Wiley, New York, 1986.
[16] S.H. Vosko, L. Wilk, M. Nusair, Can. J. Phys. 58 (1980) 1200.
[17] P.J. Stephens, F.J. Devlin, C.F. Chabalowski, M.J. Frisch, J. Phys. Chem. 98 (1994) 11623.
[18] C. Adamo, V. Barone, J. Chem. Phys. 108 (1998) 664.
[19] J.P. Perdew, K. Burke, M. Ernzerhof, Phys. Rev. Lett. 77 (1996) 3865.
[20] J.P. Perdew, K. Burke, M. Ernzerhof, Phys. Rev. Lett. 78 (1997) 1396.
[21] C. Møller, M.S. Plesset, Phys. Rev. 46 (1934) 618.
[22] B. Nielsen, A. J. Holder, GaussView, User's Reference; GAUSSIAN Inc.:

Pittsburgh, PA, 1997–1998.
[23] H. Yoshida, K. Takeda, J. Okamura, A. Ehara, H. Matsuura, J. Phys. Chem. A 106 (2002) 3580.
[24] M. H. Jamroz, VEDA Industrial Chemistry Research Institute, 8 Rydygiera Street, 01–793 Warsaw, Poland.
[25] S. Miertus, E. Scrocco, T.J. Tomasi, Chem. Phys. 55 (1981) 117.
[26] J. Tomasi, M. Persico, Chem. Rev. 94 (1994) 2027.
[27] J. Tomasi, B. Mennucci, R. Cammi, Chem. Rev. 105 (2005) 2999.
[28] C.J. Cramer, D.G. Truhlar, Chem. Res. 41 (2008) 760.
[29] M. Cossi, N. Rega, G. Scalmani, V. Barone, J. Comput. Chem. 24 (2003) 669.
[30] A.D. Laurent, D. Jacquemin, Int. J. Quantum Chem. 113 (2013) 2019.
[31] E.D. Glendening, J.K. Badenhoop, A.E. Reed, J.E. Carpenter, F.F. Weinhold, NBO 3.1 Theoretical Chemistry Institute, University of Wisconsin, Madison, WI, 1996.
[32] J.P. Foster, F. Weinhold, Natural hybrid orbitals, J. Am. Chem. Soc. 102 (1980) 7211.
[33] A.E. Reed, R.B. Weinstock, F. Weinhold, Natural-population analysis, J. Chem. Phys. 83 (1985) 735.
[34] A.E. Reed, F. Weinhold, Natural localized molecular orbitals, J. Chem. Phys. 831 (1985) 736.
[35] V. Krishnakumar, G. Keresztury, T. Sundius, R. Ramasamy, J. Mol. Struct. 702 (2004) 9.
[36] J.J.P. Stewart, J. Mol. Model. 13 (2007) 1173.
[37] M.J. Frisch, J.A. Pople, J.S. Binkley, J. Chem. Phys. 80 (1984) 3265.
[38] J.L. Duncan, Mol. Phys. 28 (1974) 1177.
[39] S. Millefiori, A. Alparone, J. Chem. Soc. Faraday Trans. 94 (1998) 25.
[40] L. Radom, W.J. Hehre, J.A. Pople, J. Am. Chem. Soc. 94 (1972) 2371.
[41] L. Radom, J.A. Pople, J. Am. Chem. Soc. 92 (1970) 4786.
[42] D. Bond, P. v. R. Schleye, J. Org. Chem. 55 (1990) 1003.
[43] N. Sadlej-Sosnowska, J. Phys. Chem. A 107 (2003) 8671.
[44] F. Trautner, A. Ben Altabef, L.E. Fernández, E. Varetti, L.H. Oberhammer, Inorg. Chem. 38 (1999) 3051.
[45] M.E. Tuttolomondo, P.E. Argarañaz, E.L. Varetti, S.A. Hayes, D.A. Wann, H.E. Robertson, D.W.H. Rankin, A. Ben Altabef, Eur. J. Inorg. Chem. (2007) 1381.
[46] M.E. Tuttolomondo, A. Navarro, E.L. Varetti, A. Ben Altabef, J. Raman Spectrosc. 36 (2005) 427.
[47] M.E. Tuttolomondo, L.E. Fernández, A. Navarro, E.L. Varetti, A. Ben Altabef, Spectrochim. Acta A 60 (2004) 611.
[48] M.E. DefonsiLestard, L.A. Ramos Guerrero, M.E. Tuttolomondo, S.E. Ulic, A. Ben Altabef, Vib. Spectrosc. 55 (2011) 153.
[49] M.E. DefonsiLestard, L.A. Ramos Guerrero, M.E. Tuttolomondo, S.E. Ulic, A. Ben Altabef, Vib. Spectrosc. 59 (2012) 40.
[50] M.F. Erben, C.O. Della Védova, R. Boese, H. Willner, C. Leibold, H. Oberhammer, Inorg. Chem. 42 (2003) 7297.
[51] B. Jasiewicz, K. Malczewska-Jaskoła, I. Kowalczyk, B. Warzajtis, U. Rychlewska, Spectrochim. Acta Part A Mol. Biomol. Spectrosc. 128 (2014) 773.